Catalysis Today 154 (2010) 61–67

Contents lists available at ScienceDirect

Catalysis Today

journal homepage: www.elsevier.com/locate/cattod

High-pressure STM study of NO reduction by CO on Pt(1 0 0)

C.T. Herbschleb, S.C. Bobaru, J.W.M. Frenken *

Kamerlingh Onnes Laboratory, Leiden University, P.O. Box 9504, 2300 RA Leiden, The Netherlands

ARTICLE INFO

Article history:
Available online 24 April 2010

Keywords:
NO-reduction
In-situ high-pressure STM
Pt(1 0 0)
Reconstruction
Langmuir–Hinshelwood kinetics

ABSTRACT

We report an investigation of the reduction of nitric oxide by carbon monoxide over a Pt(1 0 0) model catalyst at atmospheric pressure (1.25 bar). A combination has been used of high-pressure scanning tunneling microscopy and simultaneous mass spectrometry to correlate observations of the surface structure with the reaction rate and reaction mechanism. The STM images suggest that depending on the precise composition of the reactant gas mixture the Pt(1 0 0) surface switches between the quasi-hexagonal structure, characteristic for this surface in vacuum, and the bulklike (1 × 1) structure that is 20% less dense. The reaction rates that we observe are interpreted in the framework of classical Langmuir–Hinshelwood kinetics on both surface structures.

1. Introduction

Platinum is a good catalyst for many chemical reactions, such as CO oxidation and NO reduction. These are two of the three classes of reactions that take place in the three-way car catalyst, in which small, supported platinum, palladium and rhodium particles are the active elements [1–3]. In this article we concentrate on NO reduction, i.e. the conversion of nitric oxide by carbon monoxide to nitrogen and carbon dioxide. Although rhodium is the main catalyst for this reaction, the (1 0 0) surface of platinum is also known to reduce NO [4,5]. Both experimental and theoretical studies have been devoted to this reaction system. The experimental studies include temperature programmed desorption [6–8], low energy electron diffraction (LEED) [6,9,10], infrared reflection-adsorption spectroscopy [11], single-crystal adsorption calorimetry [10], scanning tunneling microscopy (STM) [12,13], X-ray photoelectron spectroscopy [14], mass spectrometry [15], molecular beam studies [8] and 3D atom probe measurements [16]. Theoretical studies include density functional theory and Monte Carlo simulations providing various models for the active sites and the reaction mechanisms [10,17–22].

Pt(1 0 0) can catalyze the complete conversion of NO and CO to N_2 and CO_2. The reaction is autocatalytic and has been proposed to be promoted by reaction intermediate species or structures like step sites [6,12].

Clean Pt(1 0 0) exhibits a surface reconstruction featuring a quasi-hexagonal monolayer on top of the square lattice below [13,20]. This reconstruction makes the top layer 20% more dense than the unreconstructed surface. The quasi-hex reconstruction is lifted by exposing the surface to adsorbates, for instance CO, O_2 and NO, adding steps to the surface by creating adatom or vacancy islands and terrace roughness [8,18,27]. At low pressures, dissociation of NO only takes place on the square lattice [7] – Pt(1 1 1) which resembles the reconstructed Pt(1 0 0) surface is not very reactive. The reaction is believed to be active above 400 K; below this temperature NO dissociation does not occur at low pressures [7,11,14,18].

Most previous experiments with surface-science techniques on the NO–CO reaction have been performed at low pressures since most of the employed techniques cannot tolerate high pressures. However, practical catalysts, such as the three-way catalyst, operate at high pressures, for example at and above atmospheric pressure. Recent studies on CO oxidation have revealed a strong pressure-gap effect between the traditional low pressures and the regime of atmospheric pressures. An alternative catalytic mechanism was identified at high pressures, accompanied by a significant change in the reaction rates [23–26]. In the light of these observations, the present study on NO reduction by CO on Pt(1 0 0) was performed at elevated temperature and atmospheric pressure.

2. Reaction kinetics

The reduction of NO by CO is believed to proceed via Langmuir–Hinshelwood (LH) kinetics, described by the following reaction equations [4,5,15,17,19,21].

$$CO_{(g)} + * \underset{k_{-1}}{\overset{k_1}{\rightleftharpoons}} CO_{(ads)} \quad (1)$$

$$NO_{(g)} + * \underset{k_{-2}}{\overset{k_2}{\rightleftharpoons}} NO_{(ads)} \quad (2)$$

* Corresponding author. Tel.: +31 71 5275603/5480; fax: +31 71 5275404.
E-mail address: frenken@physics.leidenuniv.nl (J.W.M. Frenken).

0920-5861/$ – see front matter © 2010 Elsevier B.V. All rights reserved.
doi:10.1016/j.cattod.2010.03.029

$$NO_{(ads)} + * \underset{k_{-3}}{\overset{k_3}{\rightleftharpoons}} N_{(ads)} + O_{(ads)} \tag{3}$$

$$N_{(ads)} \underset{k_{-4}}{\overset{k_4}{\rightleftharpoons}} \frac{1}{2} N_{2(g)} + * \tag{4}$$

$$CO_{(ads)} + O_{(ads)} \underset{k_{-5}}{\overset{k_5}{\rightleftharpoons}} CO_{2(g)} + 2* \tag{5}$$

We will refer to this pathway for the formation of N_2 as pathway I. An alternative pathway (II) for the creation of N_2 is:

$$NO_{(ads)} + N_{(ads)} \underset{k_{-6}}{\overset{k_6}{\rightleftharpoons}} N_2O_{(ads)} + * \tag{6}$$

$$N_2O_{(ads)} \underset{k_{-7}}{\overset{k_7}{\rightleftharpoons}} N_{2(g)} + O_{(ads)} \tag{7}$$

$$N_2O_{(ads)} \underset{k_{-8}}{\overset{k_8}{\rightleftharpoons}} N_2O_{(g)} + * \tag{8}$$

In reaction step i, k_i and k_{-i} are the rate constants for the forward and reverse directions, respectively; a free site at the surface is indicated by $*$. For this combination of reaction steps it is straightforward to derive the following equations for the formation rates of CO_2 and N_2 in the quasi-stationary regime.

$$R_{CO_2} = k_3 \frac{k_2}{k_{-2}} \frac{p_{NO}}{(1 + (k_1/k_{-1}) \cdot p_{CO} + (k_2/k_{-2}) \cdot p_{NO})^2} \tag{2.1}$$

$$\begin{aligned} R_{N_2} = {} & \frac{k_2 p_{NO}}{4k_{-2}k_4(1 + (k_1/k_{-1}) \cdot p_{CO} + (k_2/k_{-2}) \cdot p_{NO})^2} \\ & \times \left[\left(\frac{1}{2} - \frac{k_8}{k_7 + k_8} \right) k_6^2 \frac{k_2}{k_{-2}} p_{NO} \right. \\ & \left. - \left(\frac{1}{2} - \frac{k_8}{k_7 + k_8} \right) k_6 \sqrt{k_6^2 \frac{k_2^2}{k_{-2}^2} p_{NO}^2 + 8k_4k_3 \frac{k_2}{k_{-2}} p_{NO}} + 2k_3k_4 \right] \end{aligned} \tag{2.2}$$

In these equations we made the assumptions (1) that the reaction products immediately leave the surface thus $k_{-4} = k_{-5} = k_{-7} = k_{-8} = 0$, (2) that the coverages of N and O are negligibly small, (3) that NO and CO adsorption and desorption directly reach their equilibrium state, and (4) that thus the remaining reaction constants determine the overall reaction rate. The more complex structure of the formation rate for N_2 reflects the fact that it combines both pathways (reactions 4 and 7), whereas the CO_2 is only formed via pathway I (reaction 5). It is instructive to consider the N_2 formation rate in two limiting situations, namely when all N_2 is formed via the first pathway (k_4 dominant) or when all N_2 is formed via the second (k_4 negligible). In these two cases, Eq. (2.2) reduces to

$$R_{N_2} = \begin{cases} \dfrac{k_3}{2} \dfrac{k_2}{k_{-2}} \dfrac{p_{NO}}{\left(1 + (k_1/k_{-1}) \cdot p_{CO} + (k_2/k_{-2}) \cdot p_{NO}\right)^2} & k_4 \text{ dominant} \\ \dfrac{k_3k_8}{k_7 + k_8} \dfrac{k_2}{k_{-2}} \dfrac{p_{NO}}{\left(1 + (k_1/k_{-1}) \cdot p_{CO} + (k_2/k_{-2}) \cdot p_{NO}\right)^2} & k_4 \text{ negligible} \end{cases} \tag{2.3}$$

Interestingly, in each of these two limiting situations the N_2 formation rate varies with the partial pressures of NO and CO in precisely the same way, identical to the dependence of the formation rate of CO_2 on these partial pressures. We combine the relevant reaction rate constants in three parameters $K_i (i = 1, \ldots, 3)$, with which we can rewrite Eqs. (2.3) and (2.1) to

$$R_{N_2}, R_{CO_2} = K_1^{N_2,CO_2} \frac{p_{NO}}{(1 + K_2 \cdot p_{CO} + K_3 \cdot p_{NO})^2} \tag{2.4}$$

For reaction pathway I, $K_1^{N_2} = (k_3k_2/2k_{-2}) = (1/2)K_1^{CO_2}$. For reaction pathway II, $K_1^{N_2} = (k_3k_8k_2/(k_7 + k_8)k_{-2})$ and $K_1^{CO_2} = (k_3k_2/k_{-2})$ (same as for pathway I). This means that $K_1^{N_2}$ and $K_1^{CO_2}$ depend in all cases directly on the NO dissociation rate (k_3) and on the reaction constant (k_2/k_{-2}) for NO adsorption/desorption. In case of pathway II, $K_1^{N_2}$ is also determined by the ratio between the rate constants for N_2 and N_2O formation via the factor $(k_8/k_7 + k_8)$. The only difference between $K_1^{N_2}$ for the N_2 formation rates at high and low k_4 is a mere factor $(2k_8/k_7 + k_8)$. For intermediate k_4-values we are forced to return to the more complex form of Eq. (2.2). In all cases, $K_2 = (k_1/k_{-1})$ is the reaction constant for CO adsorption/desorption and $K_3 = (k_2/k_{-2})$ is the reaction constant for NO adsorption/desorption.

Since the form of the equations for R_{N_2} for both pathways and R_{CO_2} are the same, we will use this form later in an attempt to fit the experimental N_2 and CO_2 formation rates, using the K_i's as fitting parameters. As mentioned, the formation rate for CO_2 is double the first N_2 formation rate of Eq. (2.3), so that if the N_2 formation rate is dominated by the first pathway, $R_{CO_2} = 2R_{N_2}$.

We close this section by noting that a more complete description of the set of reaction rates might require the introduction of non-linear elements in one or more reaction rates, since at low pressures bi-stability and oscillations have been observed [8–10,22,28].

3. Experimental setup and sample preparation

We have conducted our experiments in a dedicated ReactorSTM™, with which model catalyst surfaces can be imaged at elevated temperatures and atmospheric pressures [23,29]. The instrument features an STM integrated with a small (0.5 ml) flow reactor cell, through which a variety of clean gas mixtures can be flown at pressures up to 2 bar. The construction of the STM-reactor combination is such that only the STM-tip and its holder are inside the reactor, while the other STM components, such as the piezo-element, are outside. The entire ReactorSTM™ system is housed in an ultrahigh vacuum (UHV) chamber. This enables us to prepare and characterize the sample surface by state-of-the-art surface-science techniques (see below). After preparation the sample is pressed firmly against the flow reactor. In that geometry it forms one of the walls of the reactor. A Kalrez ring between the sample and the rest of the reactor serves as a nearly UHV-tight seal between the reactor volume and the vacuum chamber. In order to measure the gas composition inside the reactor and thus derive the catalytic conversion rates, we take advantage of the small gas leak over the Kalrez seal into the UHV chamber, which is equipped with a quadrupole mass spectrometer (QMS). The sample holder contains a filament, located directly behind the model catalyst. With this, the sample can be heated, both for preparation purposes and during actual experiments, when the sample is placed on the reactor.

The platinum sample used in this work was a single crystal, cut and polished with the (1 0 0) surface orientation. In the UHV chamber it was prepared by multiple cycles of (1) argon ion sputtering at an ion energy of 600 eV, (2) annealing in a 1×10^{-6} mbar oxygen atmosphere at 1000 K and (3) flash annealing to a somewhat higher temperature in UHV. Low energy electron diffraction in combination with Auger electron spectroscopy was used to verify the crystalline quality and the cleanliness of the sample surface prior to transferring it to the ReactorSTM.

The flow, pressure and composition of the NO/CO gas mixture was controlled by a gas system that combined two mass flow controllers before the reactor, one for each high-purity gas, and a back-pressure controller behind the reactor. This configuration allowed us to vary the composition without changing total pressure. In our experiments the total pressure was fixed at 1.25 bar

and the flow rate was set to 8 ml_n per minute, corresponding to a refresh time of the reactor volume of 4 s.

Since CO and N_2 have the same molecular mass, 28 amu, the mass spectrometer cannot distinguish between the two directly. In order to obtain the partial pressure of the N_2 that was produced in the reaction, we combined the convoluted signal S_{28} at mass 28 with the signal S_{12} for atomic carbon (^{12}C), which is directly proportional to the partial pressure of CO.

$$p_{N_2} = c[S_{28} - nS_{12} - mS_{30}] \quad (3.1)$$

Here, c is a calibration factor relating the QMS signals to actual pressures. The factor n is a normalization constant that corrects for the sensitivity ratio between the signals at masses 28 and 12 to the partial pressure of CO. This factor was determined to be $n = 1.23$ from measurements under CO-rich conditions, when the formation rate of N_2 was negligible. Eq. (3.1) also contains a term to correct for the contamination of the NO gas used in the experiment by a trace amount of $m = 5 \times 10^{-4}$ of N_2. This contribution scales with the signal S_{30} of NO.

4. Results and discussion

4.1. STM images

In this section we present STM images taken by the ReactorSTM in different NO/CO partial pressure ratios at elevated temperatures. Fig. 1 shows STM images obtained at 382 K and 395 K in combination with the gas compositions to which the surface was exposed. The numbers in the partial-pressure graphs refer to the corresponding STM images. Image 1 is an overview of the surface when it is exposed to an NO-rich environment at 382 K, a few minutes after having been in a CO-rich mixture. The switch to the high partial pressure of NO has resulted in a high density of vacancy islands on the originally flat surface. The vacancy islands have a depth corresponding to the monatomic step height of platinum, 2.0 Å[25,30]. Images 2–4 are three consecutive images zoomed in on the area indicated by the black square in image 1. They demonstrate the high surface mobility; the vacancy islands disappear and the wavy terrace edges straighten. Image 5 is zoomed out again and it shows that the surface recovery has also taken place on a larger scale. Image 6 is the flat surface in an NO-rich environment at 395 K. Image 7 was recorded during the switch to a CO-rich environment. As can be recognized in images 7 and 8, the surface roughened under these conditions by the introduction of adatom islands and waviness in the terrace edges. Minutes later, the roughness was observed to decay as can be seen in images 9 and 10.

We interpret the changes in the STM images in terms of a surface phase transition between NO-rich and CO-rich conditions. We propose that the surface is reconstructed into the quasi-hexagonal termination when exposed to the NO-rich mixture, whereas the surface reconstruction is lifted to the (1×1) periodicity when the mixture is switched to CO-rich. We have four pieces of evidence in support of this interpretation. Firstly, the structure that we observe under NO-rich conditions differs from a surface oxide. The height differences in the images all occur as steps with the regular monatomic step height of metallic platinum, as shown in images A

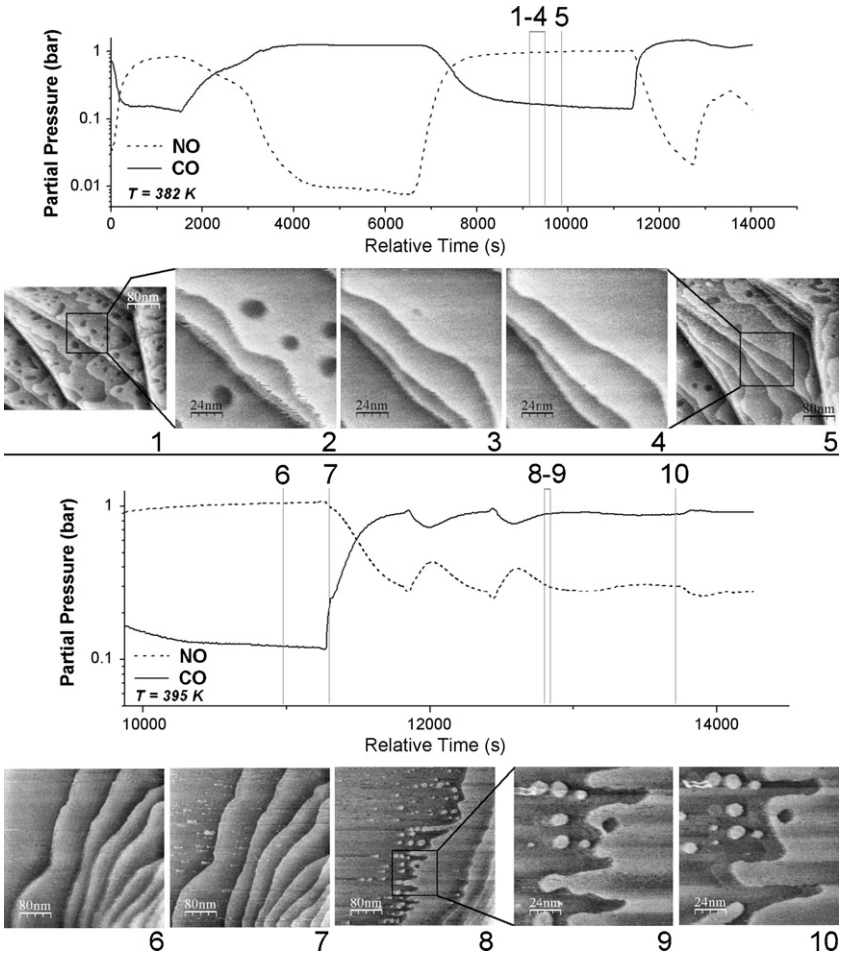

Fig. 1. Gas compositions and STM images of Pt(1 0 0) in a flowing mixture of NO/CO at a total pressure of 1.25 bar at 382 K (upper panels) and 395 K (lower panels); V_{bias} = 0.08 V; I_{tunnel} = 0.2 nA.

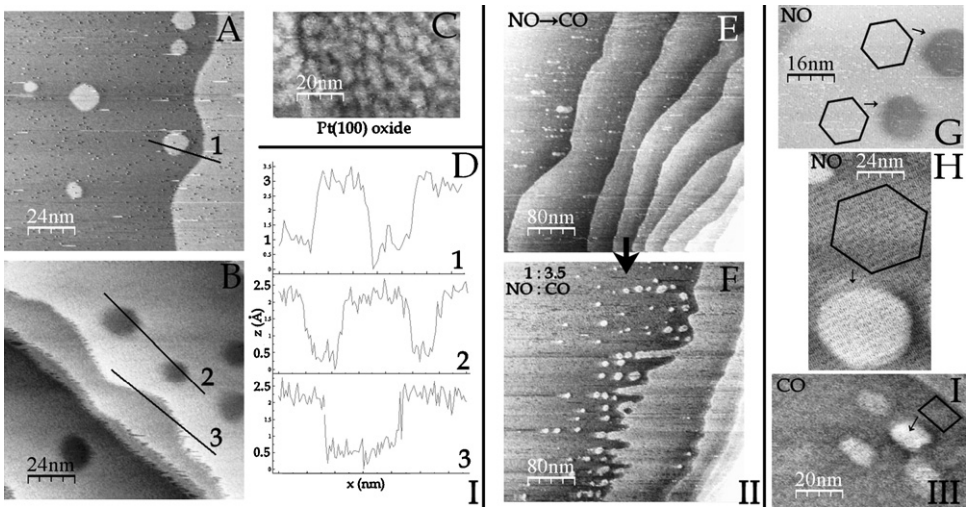

Fig. 2. Part I: Images A and B were taken in an NO-rich flow. The lines labelled 1,2 and 3 refer to the three height profiles in D, each showing height differences corresponding to the step height of Pt(1 0 0). For comparison, image C shows the roughness on this surface when it is oxidized in an O_2-rich flow. Part II: Two images illustrating the high surface mobility induced by the STM tip immediately after switching from an NO-rich to a CO-rich gas composition. Part III: STM images indicating weak hexagonal and square symmetries of vacancy and adatom islands in NO-rich and CO-rich environments, respectively.

and B and the height profiles under D in part I of Fig. 2. For comparison, in image C, we also show an image of the same surface with an oxygen-induced surface oxide, as observed in a separate experiment, where we see that oxidation makes the surface much rougher and the height variations are not quantized in units of the metallic step height. Secondly, the quasi-hex surface termination is more dense than the (1×1) lattice, implying that reconstructing the surface, starting from the unreconstructed surface, should yield vacancy islands. This is what we have indeed observed systematically, for example in Fig. 1. Similarly, de-reconstructing the surface, from quasi-hex to (1×1), should yield adatom islands, again in accordance with repeated STM observations. In both cases, after the phase transition occurred, we observed that surface diffusion slowly reduced the roughness. This shows that the observed roughness does not reflect the equilibrium structure under either the NO-rich or the CO-rich conditions; rather it should be regarded as a temporary, i.e. non-equilibrium structure, necessary to accommodate a mismatch in surface density of Pt atoms between the two structures. Thirdly, we observed that the surface temporarily responded significantly to its interaction with the STM tip when the gas composition switched from NO-rich to CO-rich, as is demonstrated in part II of Fig. 2. Image E shows the Pt(1 0 0) surface just after the switch to a CO-rich mixture. As discussed before, the switch in gas composition leads to the formation of adatom islands. In the consecutive images, such as image F of, the tip is observed to drag material over the surface, which is evidenced by the alignment of the adatom islands and the terrace roughness along the scanning direction of the STM tip (horizontal direction in all images). We believe this to be the consequence of the presence of a high density of mobile adatoms and small adatom islands, generated by the quasi-hex to (1×1) transition. This situation is temporary – after a few minutes, the surface no longer responds to the tip, while the adatom structures and the step roughness slowly decay as can be seen in the lower part of Fig. 1. Our final piece of evidence for the quasi-hex to (1×1) transition is the observation in part III of Fig. 2, that the adatom and vacancy islands exhibit a weak hexagonal symmetry in NO-rich atmospheres, as shown in images G and H, whereas the vacancy islands, observed under CO-rich conditions exhibit a weak square symmetry, as shown in image I. Our proposal of Pt(1 0 0) reconstructing in an NO-rich environment is at variance with earlier research on this reaction system, in which NO is lifting the reconstruction rather then stabilizing it [8,30]. We attribute this difference to the fact that we exposed the surface to a high (ambient) pressure of NO instead of a more traditional, low pressure of e.g. 10^{-6} mbar. In other words, this difference should be regarded as a *pressure gap* effect.

Since the surface density of the quasi-hex lattice is 20% higher than that of the (1×1) substrate lattice of Pt(1 0 0), we should expect the area of vacancy or adatom islands created upon switching gas composition to be 20% of the total area. Although our STM images are certainly consistent with this, the quality of many of our images is not sufficiently good to quantify the relative adatom or vacancy island coverage accurately. Another complicating factor is the role of the steps that can easily accommodate adatoms or vacancies and can therefore locally reduce their numbers. Furthermore, as we observed in our images, surface diffusion was efficient in quickly removing the height variations, which made only the very first images, immediately after the switching, have the full adatom or vacancy island density. Unfortunately, the characteristics moiré pattern of the hex-reconstructed Pt(1 0 0) surface [31], which we observe at room temperature and vacuum conditions, could not be resolved in NO-rich atmospheres, probably due to the NO-induced loss of image resolution.

4.2. Kinetics

In this section we concentrate on the reaction kinetics as measured with the QMS during the acquisition of the STM images. As we concluded in the previous section, the surface exhibits either a hexagonal or a square structure, depending on the ratio between the partial pressures of NO and CO. These structures are thought to be two different terminations of the metal crystal, each with its own configuration of adsorbed species. Since the surface contains no special, reacted materials such as a platinum oxide layer, we do not expect special reaction mechanisms, such as the Mars-van-Krevelen mechanism [23], and we assume that the reactions simply proceed according to LH-kinetics, under both NO-rich and CO-rich conditions. In this section we will therefore use the equations derived in Section 2 for the formation rates of N_2 and CO_2 in an attempt to fit the measured partial pressures for both cases. We emphasize that the quasi-hexagonal structure and the square (1×1) structure differ significantly, both in atom density and in geometry and symmetry. This should have an effect on the bonding geometries and the corresponding binding ener-

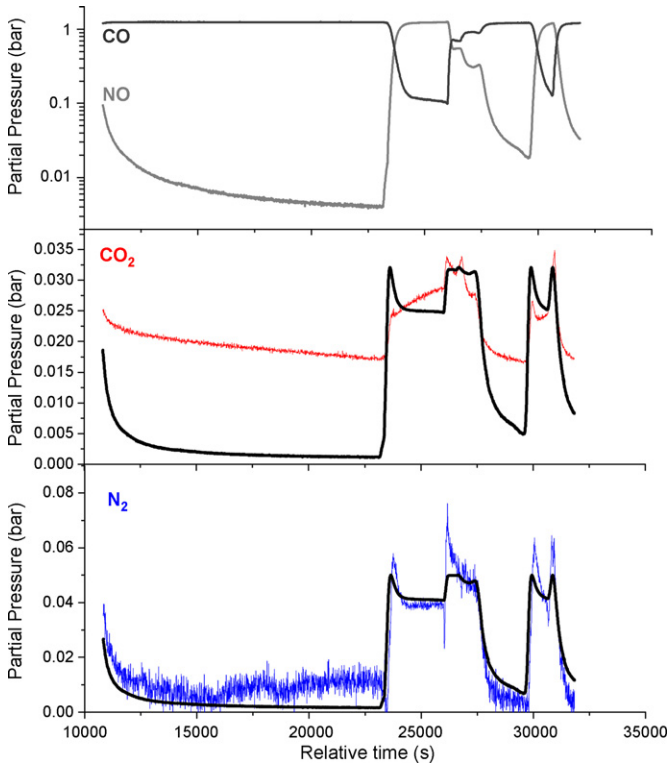

Fig. 3. Reaction rates (partial pressures) for N_2 and CO_2 production for the reactant gas mixtures shown in the upper panel. The experimental partial pressures are indicated by the red curve for CO_2 in the middle panel and by the blue curve for N_2 in the lower panel. The black curves in the lower two panels are the best-fit calculations, discussed in the text. (For interpretation of the references to color in this figure legend, the reader is referred to the web version of the article.)

gies for the reactant and product molecules on the surface and for reaction energy barriers. Such differences should be accompanied by differences in the kinetic parameters in the rate equations for both situations. Before introducing separate values for the kinetic parameters for NO-rich and CO-rich conditions, we will first attempt to fit the measurements with a single set of parameter values.

The top graph in Fig. 3 shows the CO/NO compositions to which the surface was exposed and the production of N_2 and CO_2 measured at each stage. The signatures of LH-kinetics are clearly visible in the reaction rates. The reaction rates are low in both CO- and NO-rich atmospheres and they maximize for intermediate mixtures.

In Section 2 we showed that the rate constants for the individual reaction steps combined into three fitting parameters K_i (Eq. (2.4)). Table 1 shows two sets of optimal values that we determined for these parameters by a least squares fitting procedure [32] either to the N_2 data or to the CO_2 data in Fig. 3.

Before discussing the fits in detail, we briefly address the values of the fitting parameters. We see that K_2 and K_3 have the same optimal values when fitting either N_2 or CO_2. This is in full accordance with our expectations from Section 2. The ratio between the K_1 values for the CO_2 fit and the N_2 fit is 0.7. This is much lower than the value of 2, expected when the reaction would have been dominated completely by reaction pathway I, for which $R_{CO_2} = 2R_{N_2}$. We further note that K_2 is very low, indicating that CO has a relatively strong tendency to desorb in this reaction system. By contrast, K_3, which compares the adsorption and desorption rate constants of NO, is in the order of unity.

Table 1
Optimal values for the parameters K_i, obtained separately by fitting Eq. (2.4) and its analog for CO_2 to the measured rates of N_2 and CO_2 formation in Fig. 3.

	$K_1^{N_2,CO_2}$ (cm^2/bar s)	K_2 (1/bar)	K_3 (1/bar)
N_2	0.40 ± 0.07	0.01 ± 0.01	1.95 ± 0.15
CO_2	0.29 ± 0.02	0.01 ± 0.01	2.3 ± 0.2

The LH-curves in the middle and lower panels of Fig. 3, provide reasonable fits to the measured signals. The typical LH features, such as the reaction peaks when the mixture is changing from CO-rich to NO-rich and vice versa, and also the variations of the reaction rates during more modest changes in the composition of the reactant mixture, are all reproduced, at least qualitatively, by the fits. The fit to the CO_2 signal is not as good as that for the N_2 signal. As we concluded above from the ratio between the K_1 values, N_2 production is not fully dominated by the first pathway, which implies that also N_2O has been produced. Unfortunately, the mass of N_2O, 44 amu, is equal to that of CO_2, so that their peaks in the mass spectrum add up. We further note that the extreme sharpness of the peaks in the measured N_2 signal is not represented by the fit. This discrepancy might be explained in two ways; firstly, the mass sweep of the QMS introduced systematic small differences between the precise readout times of the individual mass signals. When rapid changes occur in the partial pressures of the gasses involved in the reaction system, this may lead to a noticeable, transient error when different signals are subtracted from each other, following Eq. (3.1). Secondly, as we will discuss now, the description of the reaction rates in terms of a single set of kinetic parameters may be inadequate in view of the occurrence of two distinct surface structures.

In Section 4.1 we argued that the sudden introduction or sudden lifting of the quasi-hexagonal surface reconstruction of Pt(1 0 0) has been the cause of the surface roughness and the change in symmetry (hexagonal versus square) that were introduced upon changing from NO-rich to CO-rich gas mixtures and vice versa. Accompanying the difference between the two surface structures, we should also expect a difference in the kinetics of the NO reduction reaction. In the fits in Fig. 3 we have completely ignored this. The fact that the calculations in this figure nevertheless qualitatively fit the observations indicates that the reaction mechanism does not change, i.e. the reaction rates should be described by Langmuir–Hinshelwood kinetics for both structures, and the values for the rate constants should be quite similar. We now refine the comparison between calculated and measured reaction rates by separating the measurements in two different regimes, one corresponding to the data for which the STM observations indicate the surface to be reconstructed and the other corresponding to the unreconstructed surface. The STM images show that the two regimes correspond approximately to $p_{NO} > p_{CO}$ and $p_{NO} < p_{CO}$ respectively. For each of these two regimes we determine a separate set of values for the three parameters for the LH-kinetics.

$$R_{N_2} = \begin{cases} K_1^{hex} \dfrac{p_{NO}}{\left(1 + K_2^{hex} p_{CO} + K_3^{hex} p_{NO}\right)^2} & p_{NO} > p_{CO} \\ K_1^{(1\times1)} \dfrac{p_{NO}}{\left(1 + K_2^{(1\times1)} p_{CO} + K_3^{(1\times1)} p_{NO}\right)^2} & p_{NO} < p_{CO} \end{cases} \quad (4.1)$$

where parameters K_i^{hex} define the fit for the reconstructed surface and $K_i^{(1\times1)}$ that for the unreconstructed surface. The result of this procedure is shown in the lower panel of Fig. 4; for comparison, the upper panel repeats the best fit to the N_2 signal for the 'single-kinetics' model that was shown already in Fig. 3. The introduction of the three additional parameters has clearly led to a modest improvement of the fit. In particular, the CO-rich episodes are better described, even though the match between calculation and measurement is still not ideal.

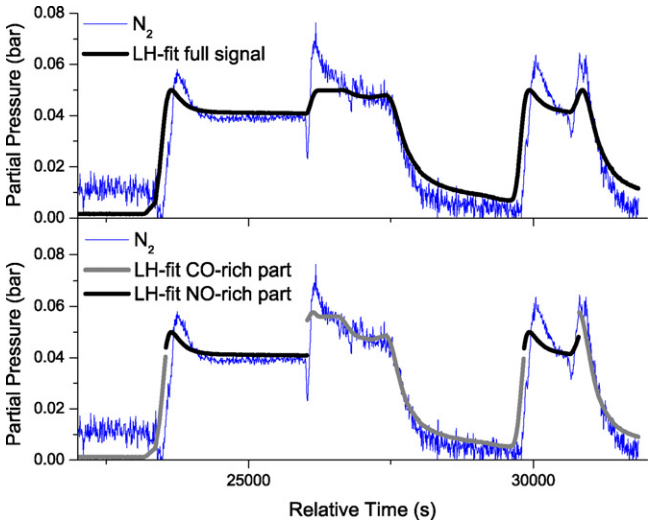

Fig. 4. (Lower panel) Fit obtained according to the dual-kinetics Langmuir–Hinshelwood model for the production of N_2, compared with the experimental N_2 signal. (Upper panel) For reference, the upper panel repeats the single-kinetics fit of Fig. 3.

The best-fit values for the six parameters of the 'dual-kinetics' model are listed in Table 2, together with the three values for the 'single-kinetics' fit.

In order to compare the quality of the fits on a more quantitative basis, we determined for both fits the normalized χ^2_ν [33].

$$\chi^2_\nu = \frac{1}{N-\nu-1}\sum_{i=0}^{N}\frac{(F_i - D_i)^2}{F_i} \tag{4.2}$$

in which N is the number of data points, ν the number of fitting parameters (either 3 or 6) and F_i and D_i are the theoretical and measured values of the reaction rate at point i. As the right column of Table 2 shows, the difference between the goodness-of-fit values for the two models is statistically insignificant. However, this is mainly due to the remaining, systematic discrepancy between the measured N_2 production rates and both models. In principle, a similar, dual-kinetics fitting procedure can be carried out for the CO_2 signal, but the quality of the fit to this signal has been relatively poor. Possibly, a full fitting procedure, involving all 16 reaction rate constants could lead to a fit with a χ^2_ν value closer to unity.

From Fig. 4 and Table 2 we extract the following information. The dual-kinetics fit for the quasi-hexagonal episodes in NO-rich mixtures is very close to the single-kinetics fit, which is also reflected in rather similar values of the three fitting parameters for the quasi-hexagonal structure and the single-kinetics model. On the other hand, as we indicated already, the fit for the square (1×1) episodes under CO-rich conditions is clearly different from, i.e. better than, the single-kinetics fit. Indeed, two of the three parameters assume somewhat different values in this case. The biggest difference can be found in K_3, the ratio between the rate constants for adsorption and desorption of NO, which is always high but tends more strongly towards NO adsorption in the quasi-hexagonal phase than in the square phase. K_1 is somewhat lower in the square phase than in the quasi-hexagonal phase, which means that either the NO dissociation step is more difficult or the N_2O production is higher in this phase.

Table 2
Optimal values of the fitting parameters for the N_2 reaction rate for the 'single-kinetics' fit (Fig. 3) and for the 'dual-kinetics' fit (Fig. 4). The units of the parameters are the same as in Table 1. The right column shows the goodness of fit, expressed as the normalized χ^2_ν, defined in Eq. (4.1).

Single kinetics	$K_1^{N_2}$	K_2	K_3	χ^2_ν
	0.40 ± 0.07	0.01 ± 0.01	1.95 ± 0.15	8.9
Dual kinetics	K_1^{hex}	K_2^{hex}	K_3^{hex}	χ^2_ν
hex	0.43 ± 0.05	0.01 ± 0.01	2.10 ± 0.20	
				9.1
	$K_1^{(1\times1)}$	$K_2^{(1\times1)}$	$K_3^{(1\times1)}$	
(1×1)	0.33 ± 0.03	0.01 ± 0.01	1.60 ± 0.10	

5. Conclusions

In this article we have investigated the reduction of NO by CO on the Pt(1 0 0) surface by in situ STM at atmospheric pressures and elevated temperatures combined with simultaneous mass spectrometry. The STM images indicate that depending on the CO:NO ratio the surface switches between two different structures, with either a square or a hexagonal symmetry, reflecting the unreconstructed (1×1) surface and the quasi-hexagonally reconstructed Pt(1 0 0) surface, respectively. We have analyzed the measured rates of N_2 and CO_2 production in terms of Langmuir–Hinshelwood kinetics. In this procedure, we have considered the possibility of two separate LH regimes, namely one for the (1×1) surface and the other for the quasi-hexagonal structure. Even though the latter, dual-kinetics fit follows the measurements more closely, the systematic differences between measurements and models are too severe to quantify this improvement.

Acknowledgements

This article is dedicated to Professor Ben Nieuwenhuys, with whom we have had the pleasure to interact frequently over the years on a wide variety of surface science and catalysis subjects. In the framework of the present article, we gratefully acknowledge Ben for fruitful discussions on our results NO reduction reactions. This research is supported by NanoNed, a technology program of the Dutch Ministry of Economic Affairs via the foundation STW.

References

[1] K.C. Taylor, Nitric oxide catalysis in automotive exhaust systems, Catal. Rev. 35 (1993) 457.
[2] M. Bowker, The Basis and Applications of Heterogeneous Catalysis, Oxford Chemistry Primers, 1998.
[3] R.M. Heck, Automobile exhaust catalysts, Appl. Catal. 221 (2001) 443.
[4] V.I. Pârvulescu, Catalytic removal of NO, Catal. Today 46 (1998) 233.
[5] B.E. Nieuwenhuys, The surface science approach toward understanding automotive exhaust conversion catalysis at the atomic level, Adv. Catal. 44 (2000) 259.
[6] M.W. Lesley, The NO + CO reaction on Pt(1 0 0), Surf. Sci. 155 (1985) 215.
[7] J.M. Gohndrome, A TPD study of NO decomposition on Pt(1 0 0), Pt(4 1 1) and Pt(2 1 1), Surf. Sci. 209 (1989) 44.
[8] A. Hopkinson, Surface restructuring dynamics in CO adsorption, desorption and reaction with NO on Pt(1 0 0), Chem. Phys. 177 (1993) 433.
[9] R. Imbihl, Bifurcation analysis of the three-variable model for the NO + CO reaction on Pt surfaces, J. Chem. Phys. 96 (1992) 6236.
[10] Y.Y. Yeo, Energetics and kinetics of CO and NO adsorption on Pt(1 0 0): restructuring and lateral interactions, J. Chem. Phys. 104 (1996) 3810.
[11] J.H. Miners, The temperature dependence of the interaction of NO + CO on Pt(1 0 0), Surf. Sci. 547 (2003) 355.
[12] W. Hösler, Defects on the Pt(1 0 0) surface and their influence on surface reactions—a scanning tunneling microscopy study, IBM J. Res. Dev. 30 (1986) 403.
[13] E. Ritter, Direct observation of a nucleation and growth process on an atomic scale, Surf. Sci. 181 (1987) 403.
[14] C.J. Weststrate, Synchrotron XPS and desorption study of the NO chemistry on a stepped Pt surface, Surf. Sci. 600 (2006).
[15] J.M.A. Harmsen, NO reduction by CO over automotive exhaust gas catalysts in the presence of O_2, Catal. Lett. 71 (2001) 81.
[16] P.A.J. Bagot, 3D atom probe study of gas adsorption and reaction on alloy catalyst surfaces. II. Results on Pt and Pt–Rh, Surf. Sci. 601 (2007) 2245.
[17] R.I. Masel, An experimental test of various models of the active site for NO reduction on platinum, Catal. Rev. 28 (1986) 335.
[18] T. Fink, The mechanism of the explosive NO + CO reaction on Pt(1 0 0): experiments and mathematical modelling, Surf. Sci. 245 (1991) 96.

[19] B. Meng, Lattice–gas model mimicking the NO + CO reaction on Pt(1 0 0), J. Chem. Phys. 101 (1994) 3234.
[20] N. Khrustova, Delay-induced chaos in catalytic surface reactions: NO reduction on Pt(1 0 0), Phys. Rev. Lett. 75 (1995) 3564.
[21] A. Eichler, NO reduction by CO on a PT(1 0 0) surface—a DFT study, J. Catal. 204 (2001) 118.
[22] S.J. Alas, Study of oscillations and pattern formation in the NO + CO reaction on Pt(1 0 0) surfaces through dynamic Monte Carlo simulation: toward a realistic model, J. Phys. Chem. B 110 (2006) 9499.
[23] B.L.M. Hendriksen, CO oxidation on Pt(1 1 0): scanning tunneling microscopy inside a high-pressure flow reactor, Phys. Rev. Lett. 89 (2002) 046101.
[24] M.D. Ackermann, Structure and reactivity of surface oxides on Pt(1 1 0) during catalytic CO oxidation, Phys. Rev. Lett. 95 (2005) 255505.
[25] S.C. Bobaru, High Pressure STM Studies of Oxidation Catalysis, Thesis, Leiden University, 2006.
[26] S.C. Bobaru et al., Mechanisms for high-pressure CO oxidation on Pt(1 0 0): Langmuir-Hinshelwood versus Mars-van Krevelen, to be published.
[27] P. van Beurden, Mechanism and dynamics of the CO-induced lifting of the Pt(1 0 0) surface reconstruction, Phys. Rev. Lett. 90 (2003) 066106.
[28] T. Fink, Kinetic oscillations in the NO + CO reaction on Pt(1 0 0): experiments and mathematical modeling, J. Chem. Phys. 95 (1991) 2109.
[29] P.B. Rasmussen, The reactor STM: a scanning tunneling microscope for investigation of catalytic surfaces at semi-industrial reaction conditions, Rev. Sci. Instrum. 69 (1998) 3879.
[30] E. Ritter, Direct observation of a nucleation and growth process on an atomic scale, Surf. Sci. 181 (1987) 403.
[31] A. Borg, STM studies of clean, CO and O_2-exposed Pt(1 0 0)-hex-R0.7°, Surf. Sci. 306 (1994) 10.
[32] Program LH-fits; EK studios (2008).
[33] P.R. Bevington, Data Reduction and Error Analysis for the Physical Sciences, McGraw-Hill, 1992.